Dalton Transactions

Accepted Manuscript

ROYAL SOCIETY OF CHEMISTRY

www.rsc.org/dalton

Cite this: DOI: 10.1039/c0xx00000x

www.rsc.org/xxxxxx

ARTICLE TYPE

Investigation of structure and ionic conductivity for intercalated kaolinites with potassium acetate in hydrous and anhydrous phases

Xiao-Pei Li,[a] Hao Yang,[a] Zheng-Fang Tian,*[a,b] Jian-Lan Liu,[a] Xiao-Ming Ren*[a,c,d]

Received (in XXX, XXX) Xth XXXXXXXXX 20XX, Accepted Xth XXXXXXXXX 20XX

DOI: 10.1039/b000000x

The intercalated kaolinite with potassium acetate (K-KAc), with *ca.* 91.9% intercalation ratio, was prepared. Thermogravimetric and variable-temperature x-ray powder diffraction analyses disclosed that a little amount of water is easily absorbed into the interlayer space of the K-KAc. The previously reported phase with the 14.2 Å interlayer distance is actually the hydrous K-KAc, which has an approximate formula of $Al_2Si_2O_5(OH)_4 \cdot 0.5KAc \cdot 0.25H_2O$. The crystal structures of hydrous and anhydrous phases of K-KAc were simulated in the density functional theory framework, demonstrating that the interactions between the K^+ and acetate ions and the inner surface of kaolinite are significantly strengthened in the anhydrous phase with regard to the hydrous phase. The ionic conductivity of K-KAc study indicated that the mobility of the interlayer ions is strongly improved by thermal activation and the conductivity increased by four orders of magnitude from 363 to 423 K.

1. Introduction

In recent years, the growing interest in renewable energy sources has led to a high demand for better and cheaper energy storage solutions, like battery systems and supercapacitors where the electrolyte is widely used.[1-4] By comparison of organic liquid electrolyte, the solid electrolyte exhibits certain advantages like improved safety, and possible higher open circuit voltages,[5-7] whereas obvious disadvantages resembling much lower ionic conductivity, and such a drawback hinders the actualization of it in an all-solid-state device.[8] To develop solid electrolytes with low cost and high ionic conductivity, the exploration, from more studies, is desirable.[9, 10]

To insert an organic salt into the interlayer of a lamellar structure material is a facile strategy for designing new type of ionic conductor, such a approach, recently, has being attracted growing attention,[11-13] besides designing and creating the microporous or open channel materials in which there exist the ions loosely binding to the framework and easily migrating.[14, 15]

Kaolinite, one of the most abundant clay mineral, is widely available on earth. It is a 1:1 phyllosilicate, characterized by a lamellar structure, with the theoretical formula $Al_2Si_2O_5(OH)_4$. The consecutive layers are connected by weak H-bond interactions and van der Waals forces between the aluminol groups of the octahedral sheet on one side, and the siloxane macrorings of the tetrahedral sheets on the other side.[16] Thus, the intercalation, the guest molecules inserted into the inter-lamellar spaces of kaolinite, is achievable.[17-21] In this context, lots of studies have focused on the investigations of the structure[22] and thermostability[23] of the intercalated kaolinites up to date, and a few of attention is being paid today to other functional properties, such as, dielectric[24] and even ferroelectrics.[20,25]

More recently, special interests have been focused on the ion conductive behaviors of the layered intercalated material because the solid-state ion conductors and/or proton conductors are widespread used in organic or inorganic nanohybrid electrode materials and usable to design novel nanoelectronic devices.[26]

In this study, we prepared the intercalated kaolinite with potassium acetate (KAc) and explored its ionic conducting behavior. We discovered, for the first time, that a little amount of water inserted into the interlayer space of anhydrous K-KAc leads to the d_{001} value obviously increasing and the previously reported phase of K-KAc with $d_{(001)}$ = 14.2 Å is actually a hydrous phase.

2. Experimental

2. 1. Materials and chemicals

Raw kaolinite (K) was obtained from Guangdong, China, with an average size of 1250 mesh, and dried at 60 °C in an airflow drying oven for 24 hours before used. Chemically pure dimethylsulfoxide (DMSO) was supplied by Sinopharm Chemical Reagent Co. Ltd. of China. All other commercially available chemicals, $KAc \cdot 0.5H_2O$ and solvents are of reagent grade and were used as received without further purification.

2. 2. Sample preparation

Preparation of intercalated kaolinite-DMSO (K-DMSO)

The intercalating precursor, K-DMSO, was synthesized according to the published procedure:[20] DMSO (9.0 mL), H_2O (1.0 mL) and kaolinite (1.0 g) were mixed at ambient temperature. The mixture was transferred to a 20 mL Teflon-lined reactor, kept at 95 °C under autogenously pressure for 6 hours, and then cooled to ambient temperature. The K-DMSO sample was filtered off, washed with absolute ethanol, and then dried at 60 °C in an airflow drying oven for 2 hours.

Preparation of intercalated kaolinite-potassium acetate (K-KAc)

The intercalated compound, K-KAc, was prepared utilizing the reported method:[27] In a beaker, KAc (8.00 g) was dissolved in 3

mL of deionized water to prepare KAc saturated solutions, and 0.20 g of K-DMSO was added to this solution. The suspension was magnetically stirred at 50 °C for 10 hours, then was separated by filtration, washed with ethanol for three times and dried at 80 °C under vacuum for 24 hours to give K-KAc solid. The efficiency of intercalation are estimated in accordance with the relative intensities of the (001) reflection originated from 'unchanged' and 'expanded' layers using Eq. (1).[28] The intercalation ratio (*I.R.*) of K-KAc was estimated to be *ca.* 91.9%.

$$I.R. = \frac{Int.(001)\ of\ \text{intercalated}\ Kaolinite}{Int.(001)\ of\ \text{intercalated}\ Kaolinite + Int.(001)\ of\ raw\ Kaolinite} \quad (1)$$

2. 3. Physical measurements

Temperature-dependent Powder X-ray diffraction (PXRD) measurements were recorded on a SHIMADZU XRD-6100 diffractometer operating with a Cu-Kα radiation source (λ = 1.5418 Å) in the temperature range from 30 to 150 °C (303–423 K). Thermogravimetric analysis (TGA) was carried out using a simultaneous NETZSCH STA 449F3 Libra between the temperature ranges of 30 and 800 °C (303-1073 K) at a rate of 10 °C/min under nitrogen atmosphere. The ionic conductivity was measured by complex impedance spectroscopy in the 1 Hz to 10^7 Hz frequency range using a Concept 80 system (Novocontrol, Germany) in the ranges between 90 and 150 °C (363–423 K) under N_2 atmosphere. The data were acquired on pellets of 78.5 mm^2 in the area and 1.74 mm in the thickness for K-KAc versus 314 mm^2 in the area and 2.4 mm in the thickness for dried raw kaolinite, with copper electrodes on the opposite surfaces of pellets. The conductivity was obtained from the resistance value obtained from the fits of Nyquist plots.

2. 4. Details for crystal structure optimization

The crystal structure optimizations were performed in the density functional theory (DFT) framework. The Cambridge sequential total energy package (CASTEP) module[29] was employed in the calculations. The total plane-wave pseudopotential method forms the basis of the CASTEP calculations. The exchange-correlation effects were treated within the generalized gradient approximation (GGA) with the Perdew-Burke-Ernzerhof functional.[30] The plane-wave basis set energy cutoff was set at 300 eV for K-KAc. The convergence parameters were set as follows: the SCF tolerance 2×10^{-6} eV/atom, the total energy tolerance 1×10^{-6} eV/atom, the maximum force tolerance 0.05 eV/Å, the maximum stress component 0.1 GPa and the displacement of convergence tolerance 0.002 Å. The other calculation parameters were set at the default values in the CASTEP code.

On basis of TG and variable-temperature PXRD measurements, it was found that a little amount of water molecules (less than 2% mass percentage) is easily absorbed into the interlayer space of the intercalated K-KAc when the dried K-KAc is exposed to air. It is interesting that the interlayer space of K-KAc was significantly expended by the inserted water molecules even if the amount of them is less. Thus, we optimized the crystal structure of K-KAc using hydrous model and anhydrous model, respectively. TG analysis revealed that the average species numbers of KAc and H_2O per unit cell are approximate 1 and 0.5, respectively. We supposed the numbers of KAc and H_2O per unit cell being one in the process of structure optimization for the hydrous phase. The starting crystal structure of the kaolinite layer in both hydrous and anhydrous phases of K-KAc was taken from the X-ray single crystal structure of the raw kaolinite at 1.5 K for optimization. On basis of the PXRD analysis, the c-axis length was fixed at c = 14.2006 Å for K-KAc·H_2O (hydrous model) and c = 11.6045 Å for K-KAc (anhydrous model), respectively; the a- and b-axes lengths as well as the α, β and γ angles are optimized.

The optimized unit cell parameters a, b, α, β, and γ are listed in Table 1 for hydrous and anhydrous phases of the intercalated K-KAc together with the reported unit cell parameters of raw kaolinite got from x-ray single crystal structure analysis.[31]

Table 1 Unit cell parameters of kaolinite from single-crystal structure analysis at 1.5 K[31] and K-KAc (hydrous and anhydrous phases) from DFT calculations

	Kaolinite[31]	Hydrous	Anhydrous
a/Å	5.1535	5.2597	5.2315
b/Å	8.9419	9.0844	9.0350
c/Å	7.3906	14.2006*	11.6045*
α/°	91.926	91.248	91.894
β/°	105.046	105.125	104.845
γ/°	89.797	90.044	89.691
V/Å^3	328.708	678.521	548.497

*The c-axis length was fixed during the optimization.

3. Results and discussion

3.1. TG analysis

The plots of raw kaolinite, K-DMSO and K-KAc are displayed in Figure 1. There is only one step of significant mass loss in the temperature range of 30-800 °C for raw kaolinite, and the onset temperature of mass loss is near 500 °C, which corresponds to the dehydroxylation of kaolinite to form metakaolinite ($Al_2O_3{\cdot}2SiO_2$). Two procedures of mass loss are observed in the TG plot of K-DMSO, and the mass loss process below 200 °C is due to the removal of inserted DMSO molecules, which onset temperature and the percentage of mass loss are consistent with the observation in literature.[32] The second mass loss process near 500 °C is attributed to the dehydroxylation of kaolinite to form metakaolinite. Two mass loss processes appeared in the temperature range of 30-800 °C for K-KAc. The mass loss process (*ca.* 1.4%) below 110 °C is attributed to the release of water absorbed in the interlayer space of kaolinite. The significant mass loss process underwent after the water completely removed, which onset temperature is *ca.* 350 °C. This procedure corresponds to the decomposition of KAc together with the dehydroxylation of kaolinite. It was noted that the process of the kaolinite dehydroxylating to form metakaolinite occurred at the same temperature in both raw kaolinite and K-DMSO, however, the KAc thermal decomposition leads to the kaolinite dehydroxylation process occurring in much lower temperature than the raw kaolinite and K-DMSO. In order to better understand the mass loss process at *ca.* 350 °C in K-KAc, the TG and DSC analyses were investigated for KAc·$0.5H_2O$ and anhydrous KAc, respectively; the corresponding TG and DSC

plots are shown in Figure S1, indicating that anhydrous KAc melts at *ca.* 298 °C and decomposes at *ca.* 430 °C to give K_2CO_3 (theoretically, with the corresponding 70% mass percentage), and the further decomposition of K_2CO_3 undergoes around 750 °C, which produced probably K_2O (theoretically, with the corresponding 47% mass percentage). It was found that no significant mass loss appears until 800 °C in the TG plot of K-KAc, demonstrating that the decomposition product of KAc in the interlayer space of kaolinite is different from K_2CO_3. Since the decomposition of KAc is coupled to the process of dehydroxylation of kaolinite, the mass loss at *ca.* 350 °C probably gave the product $Al_2O_3.2SiO_2{\cdot}xK_2O$ in K-KAc. Combining the *I.R.* value with the TG analysis,[20] the intercalated compound, K-KAc, could be represented by an approximate formula of $Al_2Si_2O_5(OH)_4{\cdot}0.5KAc{\cdot}0.25H_2O$.

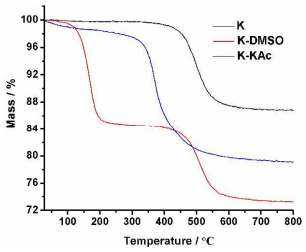

Figure 1 TG curves of raw kaolinite (K), K-DMSO and K-KAc.

3.2. PXRD and optimized crystal structures of K-KAc

The PXRD patterns of raw kaolinite, K-DMSO and K-KAc at ambient temperature are shown in Figure 2. With regard to the raw kaolinite, the 2θ value corresponding to the (001) reflection shifts towards the smaller angle in the intercalated kaolinite due to the intercalation leading to the interlayer space expansion along the c-axis. The d001 value is calculated to be 7.17 Å for K, 10.92 Å for K-DMSO and 14.20 Å for K-KAc (hydrous phase), respectively. The KAc with a little amount of water inserted into kaolinite leads to its interlayer space being increased by 7.03Å.

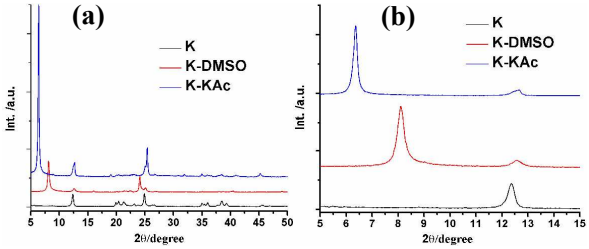

Figure 2 PXRD patterns of raw kaolinite (K), K-DMSO and K-KAc in the 2θ angles range of (a) 5-50° and (b) 5-15° at ambient temperature.

Although the as-prepared K-KAc sample was dried at 80 °C for 24 hours before PXRD measurements, it is hard to avoid that a little amount of moisture was absorbed by the sample owing to the PXRD measurements being done in air. To confirm this, the variable-temperature PXRD measurements were performed for the dried as-prepared K-KAc, and the temperature dependent PXRD profiles are shown in Figure 3. The reflection peak corresponding to the (001) crystallographic plane is almost unchanged upon heating from 313 to 333 K, while shifts towards large 2θ angle when the temperature is above 343 K (ref. Figure 3b), confirming that these water molecules are really inserted into the interlayer space of kaolinite. The PXRD pattern is recoverable when the sample was cooled down to ambient temperature and stood for over 4 hours in air. By comparison of the hydrous phase of K-KAc, the interlayer space decreases by 2.6 Å in the anhydrous phase of K-KAc. The intercalated compound of kaolinite with KAc (K-KAc) has been widely studied, and the phase with the interlayer distance of 14.20 Å was constantly thought to be anhydrous phase. This is the first time to find that (1) the intercalated compound, K-KAc, with the interlayer distance of 14.20 Å is actually a hydrous phase; (2) a little amount of water inserted into the interlayer space affects significantly the interlayer space of K-KAc.

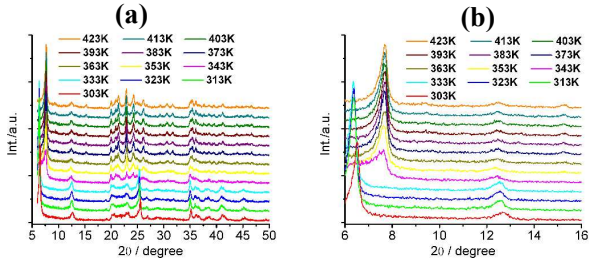

Figure 3 Temperature-dependent PXRD profiles of K-KAc with 2θ angles in the range of (a) 5-50° and (b) 6-16° (the PRXD profile at 303 K was measured when the sample cooled down for over 4 hours).

To gain more insight into the structures of both hydrous and anhydrous phases of KAc, the crystal structures were optimized using DFT method. By comparison of the reported crystal structure of kaolinite,[31] the optimized unit cell parameters (a, b, α, β and γ) in both hydrous and anhydrous phases of K-KAc are quite close to the experimental values of the raw kaolinite (see Table 1), demonstrating that the intercalation almost do not affect the atom arrangement in the intra-layer of kaolinite. The bond lengths and the bond angles of KAc in the optimized structures, together with the values obtained from the single crystal structural analyses,[34] are summarized in Table 2, indicating that the optimized bond lengths and the bond angles fall well within the ranges of the values obtained from the single crystal structure analyses.

Table 2 Bond distances (Å) and bond angles (°) in KAc

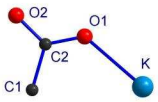

	Single crystal[34]	Hydrous model	Anhydrous model
Bond distances			
C1-C2	1.509	1.523	1.497
C2-O1	1.270	1.288	1.295
C2-O2	1.270	1.276	1.263
O1-K	2.570	2.562	2.534
Bond angles			
C1-C2-O1	117.5	116.8	118.5
C1-C2-O2	122.5	117.6	117.4
O1-C2-O2	125.0	125.6	124.0
C2-O1-K	131.0	123.1	125.7

The packing structures are displayed in Figure 4 for the hydrous and anhydrous phases of K-KAc. In the optimized crystal structure of hydrous phase K-KAc, the K^+ ion is coordinated by the O atoms from H_2O, one of acetate and

silicates, and the K-O distances, spanned from 2.636 to 3.201 Å, fall within the range of the K-O bond lengths in the reported coordination compounds of K^+ ions.[34, 35] As shown in Figure 5a, the K-O bond distances between the K^+ ion and the O atoms of silicates are much longer than that between the K^+ ion and O atoms from H_2O or acetate, indicating K^+ ions are loosely bound to the surfaces of kaolinite. There exist weakly charge-assisted H-bond interactions between the O atoms of acetates and the hydroxyl groups of gibbsite aluminol groups as well as between the O atoms of acetates and the H atoms of methyl groups. The H-bond parameters are listed in Table 3. In the optimized crystal structure of anhydrous phase K-KAc, the interlayer distance shrinks with the water releasing, this leads to the interaction between KAc and surface being strengthened, which are reflected by the H-bond parameters (ref. Figure 4b and Table 3) and the K-O distances between the K^+ ion and the O atoms of silicates (ref. Table 2).

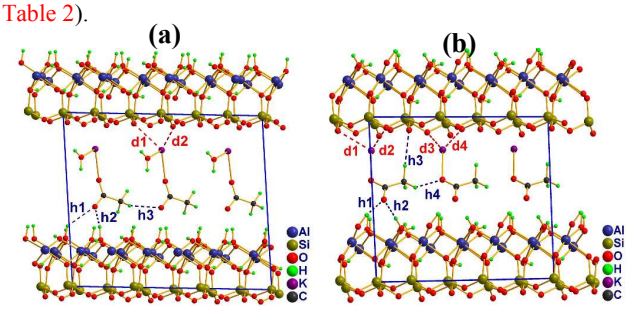

Figure 4 Packing structures viewed along the a-axis for (a) hydrous and (b) anhydrous models of K-KAc, respectively. The dotted lines represent the interatomic interactions existed in two atoms.

Table 3 Typical interatomic distances (Å) in optimized structures of hydrous and anhydrous phases of K-KAc

	Hydrous model	Anhydrous model	References
$d_{K\text{-}O}$(inner layer)			
d1	3.018	2.794	
d2	3.201	2.826	2.570[34]–3.313[35]
d3	/	3.015	
d4	/	2.860	
$d_{K\text{-}O}$(acetate)	2.562	2.534	
$d_{K\text{-}O}$(H_2O)	2.636	/	
$d_{O\text{-}H}$			
h1	2.714	1.632	
h2	1.641	1.747	
h3	2.651	2.873	Definition of the hydrogen bond[36] (IUPAC, 2011)
h4	/	2.043	
∠X-H…O[a]			
∠1	134.91	167.52	
∠2	169.70	169.47	
∠3	149.59	150.62	
∠4	/	123.89	

[a] X is referred to C or O atom, respectively.

3.3. Ionic conductivity of K-KAc

The temperature-dependent PXRD and TGA measurements disclosed that a little amount of water being residual within the interlayer space of K-KAc can be almost completely removed above 343 K, as a result, we selected the temperature range between 363 and 423 K (90-150 °C) for investigation of the impedance nature of K-KAc. The Nyquist plots are displayed in Figure 5a for the K-KAc at selected temperatures. Typically, the semicircle diameter in a Nyquist plot is directly related to the resistance of the material. In the relative low temperature region (below 373 K), the plots are almost as straight lines, indicating infinite semicircle, such a type of plot demonstrates the material possessing high resistance. The semicircle shape in the Nyquist diagram is visible and the corresponding semicircle diameter becomes smaller with increasing temperature, indicating the ionic conductivity increased at higher temperature, this is due to the thermally assisted ionic motion. Figure 5b shows the Nyquist diagrams at the selected temperatures of K-KAc at 413, 418 and 423 K, where the clear semicircle occurs at high frequencies, followed by a very small tail at low frequencies which arises from the electrode effect, signifying that the conductivity is mainly contributed from alternating current (ac) impedance rather than direct current (dc).

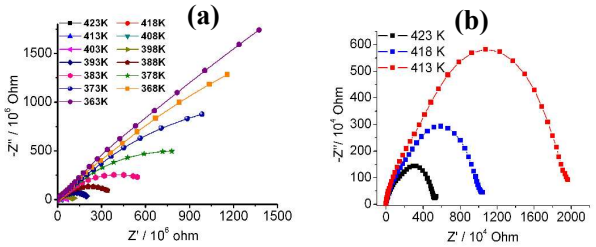

Figure 5 (a) Nyquist plots of K-KAc sample obtained at different temperature (363–423 K). (b) Close-up views of high temperature regions in the range of 413–423 K.

The ionic conductivity in K-KAc is probably contributed from two categories: (1) the migration of basic ions within the layers of kaolinite, which is called as intrinsic conduction; (2) the movement of ions inserted into the interlayer space of kaolinite (K^+ and acetate in this case), which is known as extrinsic conduction.[37] We further investigated the temperature dependent impedances of raw kaolinite, which is shown in Figure 6. The -Z'' versus Z' plots show almost straight lines in the temperature range of 293-433 K, indicating that there is absence of ionic conductivity in the selected temperature region for raw kaolinite. On the basis of above analysis, the ionic conductivity of K-KAc is attributed to the migration of K^+ and acetate ions.

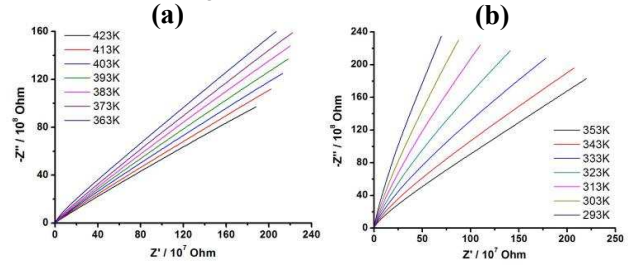

Figure 6 Nyquist plots of raw kaolinite at different temperature (a) 293 –353 K, (b) 363–423 K.

The ionic conductivity of K-KAc was further analyzed by fitting the Nyquist plots at selected temperatures. As the examples, the experimental and the fitted -Z'' versus Z' plots at

the selected temperatures of 413, 418 and 423 K are shown in Figure 7a together with the equivalent circuit, where R_1 and R_2 represent the bulk and boundary resistances (actually, two overlapped semicircles are observed in Figure 7a). The fitted bulk ionic conductivity was plotted in the form of ln(σT) vs. 1000/T, which is displayed in Figure 7b. The ionic conductivity rises drastically in the whole temperature region with increasing temperature, demonstrating that the mobility of the interlayer ions is strongly improved by thermal activation. The activation energy, E_a, was obtained utilizing the fitting the ln(σT) vs. 1000/T plot following Arrhenius equation,

$$\ln(\sigma T) = \ln A - \frac{E_a}{k_B T} \qquad (2)$$

Where the parameter A is pre-exponential factor and E_a represents the activation energy. The best fit was performed using Eq. (2) to give E_a = 2.39 eV and $\sigma = 2.8\times10^{-5}$ S/m at 423 K for K-KAc.

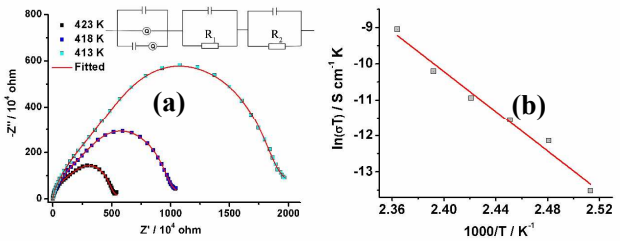

Figure 7 (a) Nyquist plots with fitted curves (Red lines), inset: Equivalent circuit diagram (b) plot of ln(σT) versus 1000/T for K-KAc (Red line is fitted one).

Conclusions

In summary, the intercalated material, K-KAc, was prepared and characterized. It is the first time to find that a little amount of water inserted into the interlayer space of anhydrous K-KAc leads to the d_{001} value obviously increasing and the previously reported phase of K-KAc with $d_{(001)}$ = 14.2 Å is actually a hydrous phase. The ionic conductivity of K-KAc was investigated, indicating that the σ value increases by four orders of magnitude from 373 K to 423 K owing to the mobility of ions (K^+ and acetate ions) located in the interlayer space being thermally activated. This study provides a strategy to design new solid electrolytes via insertion of organic salt into the lamella minerals or the MOFs with pores or channels.

Acknowledgments

The authors thank the Priority Academic Program Development of the Jiangsu Higher Education Institutions and the National Nature Science Foundation of China (Grant no. 91122011 and 21271103) for financial support.

Notes and references

[a] *State Key Laboratory of Materials-Oriented Chemical Engineering and College of Science, Nanjing Tech University, Nanjing 210009, P. R. China. Fax: 86-25-58139481; Tel: 86-25-58139476; E-mail: xmren@njtech.edu.cn*

[b] *School of Chemical Engineer, Huanggang Normal University, Huanggang 438000, P. R. China*

[c] *College of Materials Science and Engineering, Nanjing Tech University, Nanjing 210009, P. R. China*

[d] *Coordination Chemistry Institute & State Key Laboratory, Nanjing University, Nanjing 210093, P. R. China*

† Electronic Supplementary Information (ESI) available: TG of hydrous KAc·0.5H_2O and anhydrous KAc, Experimental and calculated PXRD patterns of hydrous and anhydrous models and Calculated resistances of boundary and block. See DOI: 10.1039/b000000x/

‡ **Xiao-Pei Li and Hao Yang contribute equally.**

1. X. Xu, K. Takada, K. Watanabe, I. Sakaguchi, K. Akatsuka, B.-T. Hang, T. Ohnishi and T. Sasaki, *Chem. Mater.*, 2011, **23**, 3798.
2. P. Lacorre, F. Goutenoire, O. Bohnke, R. Retoux and Y. Laligant, *Nature*, 2000, **404**, 856.
3. L.-L. Zhang and X.-S. Zhao, *Chem. Soc. Rev.*, 2009, **38**, 2520.
4. H.-Y. Lee and J.-B. Goodenough, *J. Solid State Chem.*, 1999, **144**, 220.
5. J.-B. Goodenough and K.-S. Park, *J. Am. Chem. Soc.*, 2013, **135**, 1167.
6. J.-M. Tarascon and M. Armand, *Nature*, 2001, **414**, 359.
7. Y. Shao, F. Ding, J. Xiao, J. Zhang, W. Xu, S. Park, J.-G. Zhang, Y. Wang and J. Liu, *Adv. Funct. Mater.*, 2013, **23**, 987.
8. N. Kamaya, K. Homma, Y. Yamakawa, M. Hirayama, R. Kanno, M. Yonemura, T. Kamiyama, Y. Kato, S. Hama, K. Kawamoto and A. Mitsui, *Nat. Mater.*, 2011, **10**, 682.
9. X.-Y. Dong, R. Wang, J.-B. Li, S.-Q. Zang, H.-W. Hou and T. C. W. Mak, *Chem. Commun.*, 2013, **49**, 10590.
10. R. Wang, X.-Y. Dong, H. Xu, R.-B. Pei, M.-L. Ma, S.-Q. Zang, H.-W. Hou and T. C. W. Mak, *Chem. Commun.*, 2014, **50**, 9153.
11. (a) S. Letaief, P. Aranda and E. R. Hitzky, *Appl. Clay. Sci.*, 2005, **28**, 183; (b) P. Aranda, E. R. Hitzky, *Appl. Clay. Sci.*, 1999, **15**, 119; (c) J. C. Galvan, A. J. Morales, R. Jimenez, J. Merino, A. Villanueva, M. Crespin, P. Aranda and E. R. Hitzky, *Chem. Mater.*, 1998, **10**, 3379.
12. D. M. M. Krishantha, R. M. G. Rajapakse, D. T. B. Tennakoon and H. V. R. Dias, *Ionics*, 2006, **12**, 287.
13. S. Letaief, T. Diaco, W. Pell, S. I. Gorelsky and C. Detellier, *Chem. Mater.*, 2008, **20**, 7136.
14. N. F. Zheng, X. H. Bu and P. Y. Feng, *Nature*, 2003, **426**, 428.
15. X.-Y. Dong, R. Wang, J.-Z. Wang, S.-Q. Zang and T. C. W. Mak, *J. Mater. Chem. A*, 2015, **3**, 641.
16. (a) H. H. Murray, S. W. Bailey, *Miner. Soc. Amer.: Chelsea, MI*, 1991, Vol. 19, pp 67; (b) H. H. Murray, W. Bundy, C. Harvey, *Clay Miner. Soc.: Boulder, CO*, 1993.
17. (a) J. G. Thompson and C. Cuff, *Clays Clay Miner.*, 1985, **33**, 490; (b) P. J. R. Uwins, I. D. R. Mackinnon, J. G. Thompson and A. J. E. Yago, *Clays Clay Miner.*, 1993, **41**, 707; (c) J. J. Tunney and C. Detellier, *Chem. Mater.*, 1996, **8**, 927; (d) T. A. Elbokl and C. Detellier, *J. Phys. Chem. Solids*, 2006, **67**, 950.
18. G. Z. Zou, H. Gao, J. L. Liu, S. P. Zhao, Z. F. Tian and X. M. Ren, *RSC Adv.*, 2013, **3**, 23596.
19. Q. Qiao, H. Yang, J. L. Liu, S. P. Zhao and X. M. Ren, *Dalton Trans.*, 2014, **14**, 5427.
20. S. P. Zhao, H. Gao, X. M. Ren, G. J. Yuan and Y. N. Lu, *J. Mater. Chem.*, 2012, **22**, 447.
21. R. Frost, J. Kristof, E. Mako and J. T. Kloprogge, *Langmuir*, 2000, **16**, 7421.
22. M. Gábor, M. Tóth, J. Kristóf and G. Komáromi-Hiller, *Clays Clay Miner.*, 1995, **43**, 223.
23. (a) M. Gabor, M. Toth, J. Kristof and G. Komaromi-Hiller, *Clays Clay Miner.*, 1995, **43**, 223; (b) C. E. White, J. L. Provis, L. E. Gordon, D. P. Riley, T. Proffen and S. J. Jannie, *Chem. Mater.*, 2011, **23**, 188.
24. K. Orzechowski, T. Słonka and J. Głowinski, *J. Mater. Chem. Solids*, 2006, **67**, 915.
25. T. Croteau, A. K. Bertram and G. N. Patey, *J. Phys. Chem. A*, 2010, **114**, 8396.
26. (a) I. K. Tonle, S. Letaief, E. Ngameni and C. Detellier, *J. Mater. Chem.*, 2009, **33**, 5996; (b) G. K. Dedzo, S. Letaief and C. Detellier, *J. Mater. Chem.*, 2012, **22**, 20593; (c) L. Wang, Z. H. Dong, Z. G. Wang, F. X. Zhang and J. Jin, *Adv. Funct. Mater.*, 2013, **23**, 2758.

27. R. L. Frost, J. Kristof, E. Mako and W. N. Martens, *Langmuir*, 2002, **18**, 6491.
28. R. L. Ledoux and J. L. White, *Science*, 1964, **143**, 244.
29. M. D. Segall, P. J. D. Lindan, M. J. Probert, C. J. Pickard, P. J. Hasnip, S. J. Clark and M. C. Payne, *J. Phys.: Condens. Matter,* 2002, **14**, 2717.
30. J. P. Perdew, K. Burke and M. Ernzerhof, *Phys. Rev. Lett.*, 1996, **77**, 3865.
31. R. L. Frost, O. B. Locos, J. Kristof and J. T. Kloprogge, *Vib. Spectrosc.*, 2001, **26**, 33.
32. R. A. Miranda, J. Llorca, F. Medina, J. E. Sueiras and A. M. Segarra, *J. Catal.*, 2011, **282**, 65.
33. R. L. Frost, J. Kristof, E. Horvath and J. T. Kloprogge, *J. Colloid Interface Sci.*, 1999, **214**, 109.
34. R. L. Lin, W. Q. Sun, Y. F. Hu, W. R. Yao, H. L. Zhu and J. X. Liu, *Supramol. Chem.*, 2011, **23**, 829.
35. (a) T. A. Hanna, L. H. Liu, A. M. Angeles-Boza, X. D. Kou, C. D. Gutsche, K. Ejsmont, W. H. Watson, L. N. Zakharov, C. D. Incarvito and A. L. Rheingold, *J. Am. Chem. Soc.,* 2003, **125**, 6228; (b) S. Burnet, A. K. Hall, J. M. Harrowfield, G. A. Koutsantonis, V. Sanford, D. Sauter, B. W. Skelton, A. H. White, *Supromol. Chem.,* 2003, **15**, 291; (c) W. H. Yu, X. Z. Wang, Y. X. Sui, X. M. Ren, Q. J. Meng, *Inorg. Chem. Comm.,* 2008, **11**, 799.
36. E. Arunan, G. R. Desiraju, R. A. Klein, J. Sadlej, S. Scheiner, I. Alkorta, D. C. Clary, R. H. Crabtree, J. J. Dannenberg, P. Hobza, H. G. Kjaergaard, A. C. Legon, B. Mennucci and D. J. Nesbitt, *Pure Appl. Chem.,* 2011, **83**, 1637.
37. J. Halbritter, *Phys. Rev. B*, 1993, **48**, 9735.